Orientation Profiles in the Strand of Thermotropic Liquid-Crystalline Polymer Studied by Polarized Fourier Transform Infrared Microspectroscopy

A. Kaito,* M. Kyotani, and K. Nakayama

Research Institute for Polymers and Textiles, 1-1-4, Higashi, Tsukuba, Ibaraki 305, Japan

Received September 18, 1990; Revised Manuscript Received December 17, 1990

ABSTRACT: The orientation profiles in extrusion-molded strands of a thermotropic liquid-crystalline polyester were obtained by Fourier transform infrared (FTIR) microspectroscopy. The polarized infrared spectra were measured in microscopic area down to 40 μm as a function of distance from the centers of the strands. The orientation profiles are discussed in relation to the morphological structure studied by polarized optical microscopy and scanning electron microscopy (SEM). In the case of the strand 1.52 mm thick, the microscopic orientation function is lower in the central region of the strand but increases markedly toward the surface of the strand. The core region of the thicker strand exhibits curved band patterns in polarized optical micrography and scanning electron micrographs. With decreasing strand diameter, the microscopic orientation function varies more gradually with the radial position and the orientation function in the central region is much improved. The fracture surface of thinner strands does not show a band pattern but exhibits highly oriented fibrillar morphology.

Introduction

Over the last decade, thermotropic liquid-crystalline polymers have attracted the interest of many researchers because they can be processed into high-performance materials. In the molding process, the molecular chains tend to follow the direction of the polymer melt flow. As a result, the fabrics of liquid-crystalline polymers exhibit high stiffness and high strength in the flow direction. A number of studies has been reported on fiber spinning from the nematic phase of thermotropic liquid-crystalline polymers.[1-7] The liquid-crystalline polymers were also fabricated into rods and bars with larger cross sections by means of extrusion[8-11] and injection[12-14] moldings. In these studies, the mechanical properties and the microstructures were extensively studied in relation to the flow characteristics of the mesophase melts.

It is also known that the liquid-crystalline polymers have a skin–core structure with a highly oriented skin layer and a less oriented core region. The skin–core structures were confirmed by morphological observations using the scanning electron microscope (SEM) and the polarized optical microscope.[2,9-12] The radial distribution of molecular orientations was studied for the extrusion-molded rods by means of wide-angle X-ray diffraction[1,8,10] and birefringence.[1,9] Microbeam X-ray diffraction with a 100-μm beam diameter was applied to evaluation of the microscopic orientation function in injection-molded plaques of liquid-crystalline polymers.[13] The ATR dichroism technique was used to obtain the orientation profiles in injection-molded plaques of a liquid-crystalline polymer.[14] In spite of extensive studies, the structural profiles were obtained mainly for fibers with larger cross section because of the limitation of the spatial resolution of the analytical procedures.

Recently there has been marked progress in Fourier transform infrared (FTIR) microspectroscopy as a tool for the microscopic analysis.[15-22] By a combination of FTIR spectroscopy with optical microscopy, high-quality infrared (IR) spectra can be obtained for the microscopic area that is determined by the IR microscope. Therefore, FTIR microspectroscopy provides valuable information on the molecular structure in the microscopic domain down to 10 μm. Because of the gain in spatial resolution, FTIR microspectroscopy has been extensively used for analyzing small areas, such as contaminants or inhomogeneities in materials,[16] thin fibers,[15,17,20] and thin layers in the laminated films.[18,20]

In this work, polarization measurements by FTIR microspectroscopy are applied to characterize the microscopic orientation in extrusion-molded strands of a thermotropic liquid-crystalline polymer. In addition, the orientation distribution studied by FTIR microspectroscopy is correlated with the mechanical properties and the morphological observations.

Experimental Section

Sample Preparation. The sample studied in this work is a liquid-crystalline copolyester consisting of 73 mol % of *p*-hydroxybenzoic acid (HBA) and 27 mol % of 2-hydroxy-6-naphthoic acid (HNA). The polymer exhibits a crystal–mesophase transition at 278 °C. Pellets of the copolyester were obtained from the Polyplastics Co., Ltd. The strands were extruded using a single-screw extruder equipped with a conical die, after the pellets of the polymer were dried at 90 °C for 12 h and 120 °C for 3 h. The diameter of the die outlet D was varied in the range of 1–4 mm, and the value of L/D, the length-to-diameter ratio of the die orifice, was set at 2 or 5. The die temperature was controlled at 310 ± 2 °C. After leaving the die outlet, the strands were further drawn down and slowly cooled to ambient temperature.

Characterization. Sonic velocity was measured at a frequency of 10 kHz by using a pulse propagation meter, Rheovibron DDV-5-B (Orientec Corp.). A tensile load of 100–130 g was applied to the sample during the measurement of sonic velocity. The sonic modulus was calculated from the sonic velocity and density. Density was measured with a carbon tetrachloride–*n*-heptane density gradient column at 25 °C.

The crystal orientation function in the bulk was determined from the azimuthal intensity distribution of wide-angle X-ray diffraction (WAXD). Ni-filtered Cu Kα radiation generated by a Geiger Flex XGC-20 (Rigaku Denki Co., Ltd.) was used as an incident X-ray beam. The WAXD intensity was measured by using a scintillation counter and a pulse height analyzer.

The strands were microtomed in the extrusion direction to a thickness of 10 μm after the strands were embedded in an epoxy resin. The microtomed sections were characterized by polarized optical microscopy and polarized FTIR microspectroscopy.

The polarized optical micrographs were taken with a polarizing microscope under crossed polarizers in the diagonal direction. The photographs were taken with a 35-mm camera.

0024-9297/91/2224-3244$02.50/0

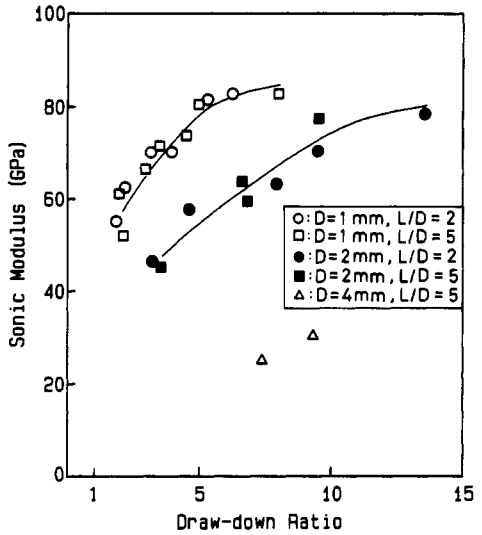

Figure 1. Sonic modulus of the liquid-crystalline polymer as a function of draw-down ratio.

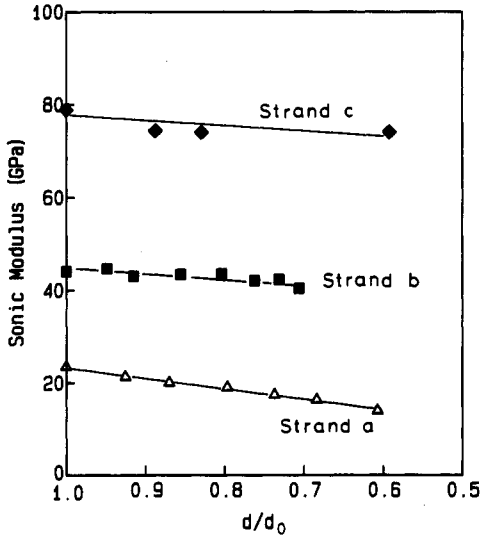

Figure 2. Variation of sonic modulus with the ratio of diameter, d/d_0, after and before scraping.

The FTIR microspectra were measured on a Perkin-Elmer Model 1800 FTIR spectrometer equipped with a liquid-nitrogen-cooled MCT detector; 500–1000 scans of 4-cm^{-1} resolution were averaged to obtain a sufficient signal-to-noise ratio. The microbeam radiation was obtained with a redundantly apertured infrared microscope, IR plan Model 100 (Spectra-Tec, Inc.). The microscope area for the spectral analysis was defined by two apertures, one before and another after the specimen. Infrared radiation was focused on the sample using a 15× Cassegrain objective, after passing through the first aperture. A slit of 0.6–1.2 mm wide and 3 mm long was used for the first aperture, so as to form a sample image with a 40–80 μm × 200 μm dimension. The transmitted IR beam was transferred to the spectrometer by a 10× condenser, and the area of its image plane was masked again by the second aperture. In order to produce the polarized radiation, a wire-grid polarizer was placed under the condenser. The polarized FTIR spectrum was obtained by changing the polarization direction of the polarizer.

The fracture surfaces were observed by scanning electron microscopy (SEM). The strands were fractured in the extrusion direction at liquid-nitrogen temperature.

Results

Mechanical Properties. Figure 1 shows the dependence of the sonic modulus upon the draw-down ratio for each diameter of die. The sonic modulus increased with increasing draw-down ratio. The increase of sonic modulus tended to saturate at higher draw-down ratios when the diameter of the die outlet, D, was 1 mm. For a given draw-down ratio, the sonic modulus increased with a decrease in the diameter of the die outlet. The length-to-diameter ratio, L/D, of the die outlet did not have any significant effect on the sonic modulus.

Table I
Characteristics of Selected Strands

sample	D,[a] mm	draw-down ratio	d_0,[b] mm	bulk orientation function
strand a	4	7.0	1.52	0.676
strand b	2	3.2	1.12	0.812
strand c	2	10.2	0.63	0.879

[a] Diameter of die outlet. [b] Diameter of strand.

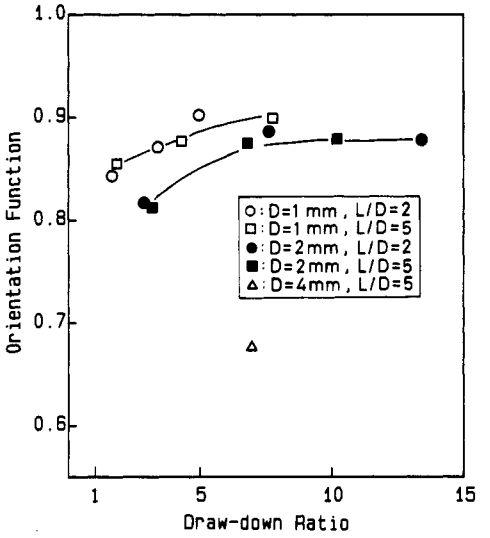

Figure 3. Bulk orientation function of the liquid-crystalline polymer determined by WAXD as a function of draw-down ratio.

In order to study the dependence of the mechanical properties on the radial position, the sonic modulus was measured by scraping the surface layer of the strands. Figure 2 shows the variations of sonic modulus with the ratio of the diameter, d/d_0, after and before scraping. The processing conditions of the three strands shown in Figure 2 are summarized in Table I. Strand a was extruded from a conical die 4 mm in diameter, while strand b and strand c were obtained by using a conical die 2 mm in diameter. Strand c was taken up at a higher velocity than strand b. The sonic wave tends to propagate near the surface of samples, because its amplitude attenuates inside the polymeric materials. Therefore, the variation of sonic modulus with scraping represents approximately the distribution of the modulus in the radial direction. The sonic modulus decreased markedly with decreasing d/d_0 for the thicker strand (strand a), while the sonic modulus was relatively constant in the radial direction for the thinner strand (strand c).

Bulk Orientation Function. The second moment of the crystal orientation function was obtained from the azimuthal intensity distribution of the meridional WAXD reflection observed at $2\theta = 42.8°$. Although the strands of liquid-crystalline polymers are expected to have an orientation distribution inside the sample, the orientation function obtained from WAXD represents the orientation function averaged over the sample. Figure 3 shows the dependence of the bulk orientation function on the draw-down ratio. The orientation function increased with increasing draw-down ratio and with decreasing diameter

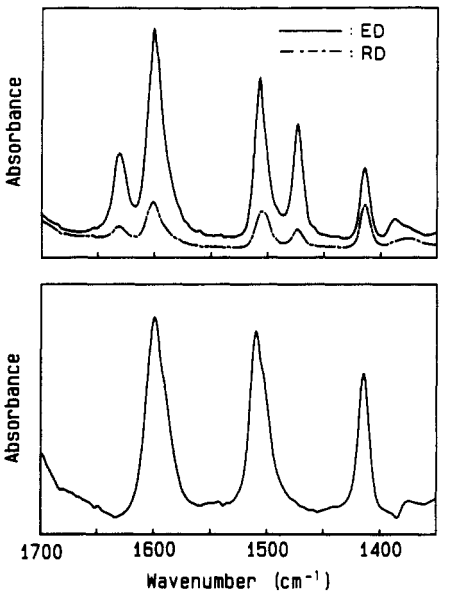

Figure 4. Comparison of the FTIR microspectra of HBA/HNA copolymer (upper) with the diffuse reflection spectrum of HBA homopolymer (lower) in the spectral region of 1700–1350 cm^{-1}.

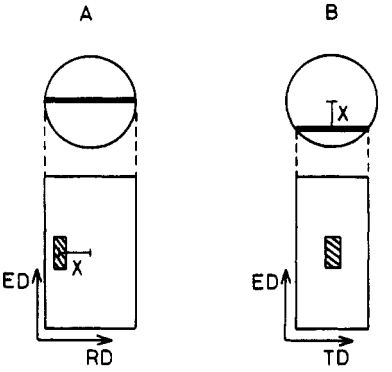

Figure 5. Microtomed section of the strand used for the measurements of FTIR microspectroscopy.

of the die outlet, which parallels the dependence of the sonic modulus on the processing variables.

Orientation Profiles Obtained by FTIR Microspectroscopy. The FTIR spectra in the wavenumber region of 1700–1350 cm^{-1} are shown in Figure 4. The polarized FTIR spectra in the microscopic area of strand c are shown in the upper part of the figure. A sufficient signal-to-noise ratio was achieved for the 40 $\mu m \times 200$ μm aperture by averaging 1000 scans of 4-cm^{-1} resolution.

In order to discuss the spectral assignments, the diffuse reflection spectrum of the powder of the HBA homopolymer is also given in the lower part of Figure 4. Powders of the homopolymer were ground and dispersed in KBr powder at about 1% concentration. The absorbance spectrum was obtained from the diffuse reflectance by use of the Kubelka–Munka equation.

The CC stretching vibrations of the aromatic rings were observed in this spectral region and exhibited parallel dichroism. By referring to the spectrum of homopolymer, the IR bands at 1415, 1506, and 1632 cm^{-1} are assigned to the skeletal vibration of the benzene ring while those at 1474 and 1602 cm^{-1} are ascribed to that of the naphthalene ring.

The specimen microtomed from the central part of the strand is shown in Figure 5A. The polarized FTIR spectra were measured by changing the distance, X, from the center of the microtomed specimen. Measurements were also carried out for the central part of the section that was

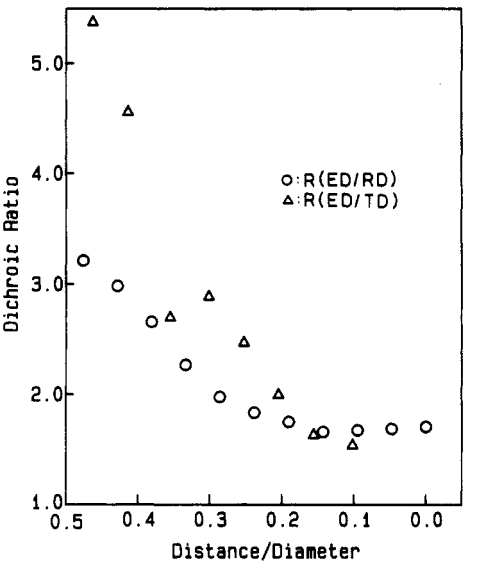

Figure 6. Orientation profile of strand a obtained from the 1474-cm^{-1} band; dimension of sample image = 80 × 200 μm; number of scans = 500.

microtomed at the position X from the center of the strand (Figure 5B). The measurement shown in Figure 5A gives the spectra polarized in the extrusion direction (ED) and in the radial direction (RD), whereas the dichroic spectra in the extrusion direction and the tangential direction (TD) were obtained in the way shown in Figure 5B.

The radial profiles of molecular orientation were obtained for the three strands whose characteristics were shown in Table I. Figure 6 shows the orientation profile of strand a, which was obtained by plotting the dichroic ratio of the 1474-cm^{-1} band (skeletal vibration of the naphthalene ring) against the distance from the center of the strand. The circles stand for the ratio of absorption intensity in the extrusion and radial directions, R(ED/RD), and the triangles represent the dichroic ratio in the extrusion and tangential directions, R(ED/TD). In the central region of the strand ($X/d_0 < 0.2$), the dichroic ratio was as low as 1.4–1.8. From the center to the surface, however, the dichroic ratio markedly increased and the molecular orientation became displaced from the uniaxial orientation (R(ED/TD) > R(ED/RD)). In the surface region, the molecular chains were highly oriented to ED, and the fraction of the TD orientation was less than that of the RD orientation.

Figure 7 shows the orientation profile of strand a obtained from the 889-cm^{-1} band, which is assigned to the CH out-of-plane bending vibration of the benzene ring. As the transition moment direction of this vibration is perpendicular to the benzene ring and thereby to the fiber axis, the value of the dichroic ratio decreases with an increase in the degree of molecular orientation. The molecular chains were highly oriented in ED near the surface but less oriented in the center. Judging from the similarity of the orientation profile obtained from the 889-cm^{-1} band to that obtained from the 1474-cm^{-1} band, the HBA and HNA units seem to orient in the extrusion direction in an analogous way. The result parallels the random sequence structure of this copolyester.

Figure 8 shows the orientation profile of strand b determined by the dichroic ratio of the 1474-cm^{-1} band. Although the dichroic ratio in the surface region was still higher than that in the central region, the dichroic ratio in strand b more gradually varied with position than that in strand a. The orientation function in the central region markedly increased in strand b as compared with strand

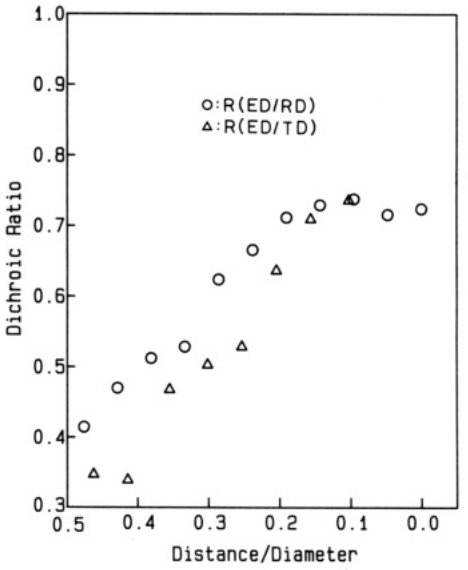

Figure 7. Orientation profile of strand a obtained from the 889-cm^{-1} band; dimension of sample image = 80 × 200 μm; number of scans = 500.

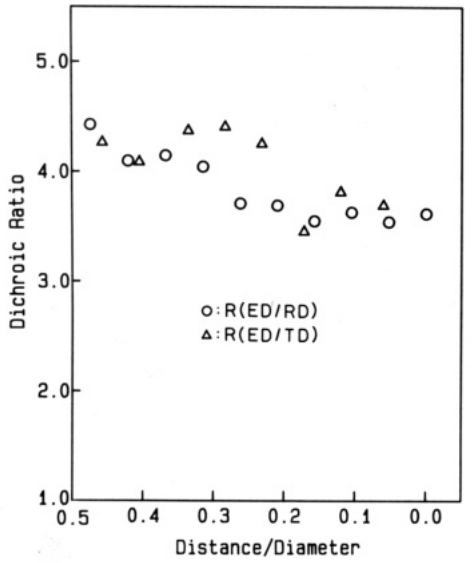

Figure 8. Orientation profile of strand b obtained from the 1474-cm^{-1} band; dimension of sample image = 60 × 200 μm; number of scans = 700.

a. In contrast to strand a, the mode of molecular orientation in strand b was approximated by the uniaxial orientation to ED.

Figure 9 shows the orientation profile of strand c obtained from the 1474-cm^{-1} band. Although the values of the dichroic ratio were somewhat scattered, it did not show any systematic dependence upon radial position. The orientation function in strand c was shown to be higher than that in strand a and strand b, at any position from center to skin.

Morphological Observation. Figure 10 shows the polarized optical micrograph of the microtomed section of strand a. The central region exhibited a band pattern consisting of dark and bright layers perpendicular to ED. The interval of the banded layers was several micrometers. On approaching the surface, however, the band pattern was curved and the striation became parallel to ED at about 100 μm from the surface. A surface layer 100 μm thick seems to be homogeneous without showing the band pattern.

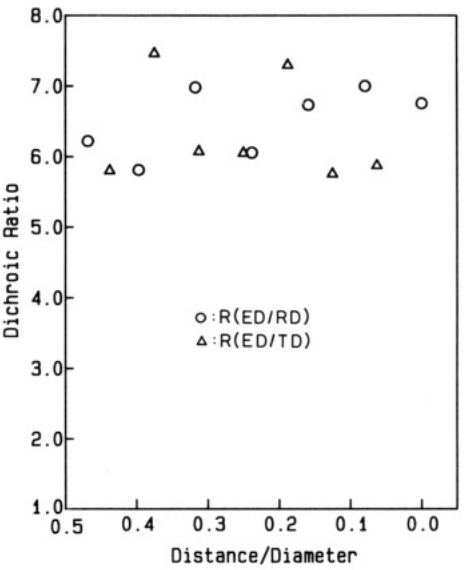

Figure 9. Orientation profile of strand c obtained from the 1474-cm^{-1} band; dimension of sample image = 40 × 200 μm; number of scans = 1000.

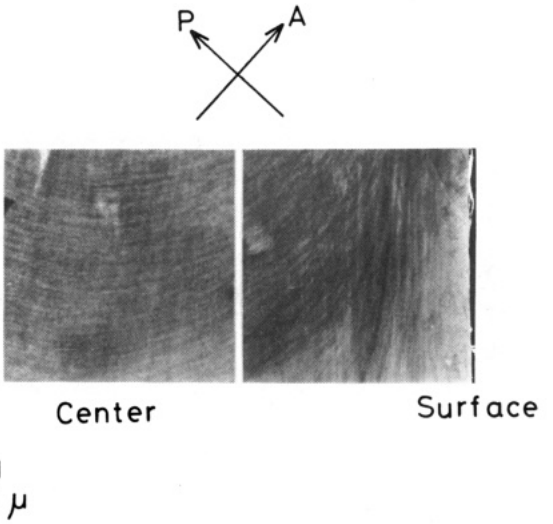

Figure 10. Polarized optical micrograph of strand a.

The band pattern was observed also in the SEM photographs of the fracture surface of strand a, which is shown in Figure 11. In the magnified view, we observed short wavelike fibrils whose axes were distributed around the extrusion direction. The wavy fibrils were aligned in the transverse direction, forming a layered texture. The length of the short fibrils was 4–6 μm and was in coincidence with the pitch of the band pattern observed in the polarized optical micrograph.

Figure 12 shows the polarized optical micrographs of thin sections of strand b and strand c. In contrast to strand a, the core region of strand b and strand c did not exhibit any band pattern, suggesting that the structure in these thin strands was relatively homogeneous along the extrusion direction.

The fracture surface morphology of the central region of strand b is shown in Figure 13. Although the morphology of strand a was not subdivided into thin fibers, strand b was configured in aggregation of straight fibrils ranging from 1 to 5 μm in diameter. The fibrils in strand b were highly oriented in the extrusion direction.

Discussion

Validity of FTIR Microspectroscopy. The quality of the FTIR microspectrum was reported to depend upon

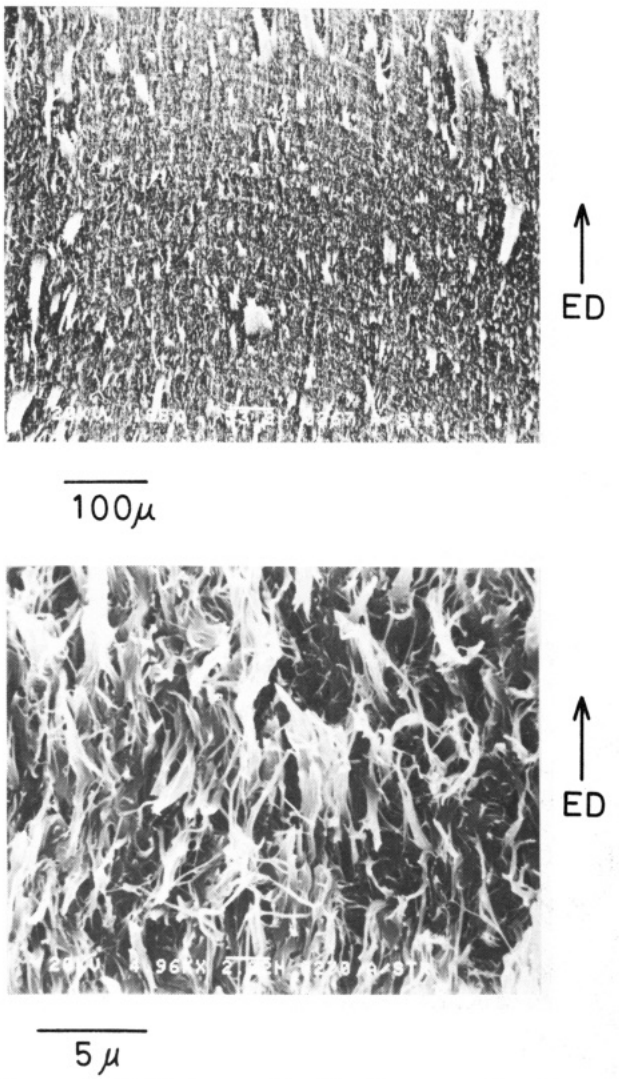

Figure 11. SEM photographs of the fracture surface of strand a.

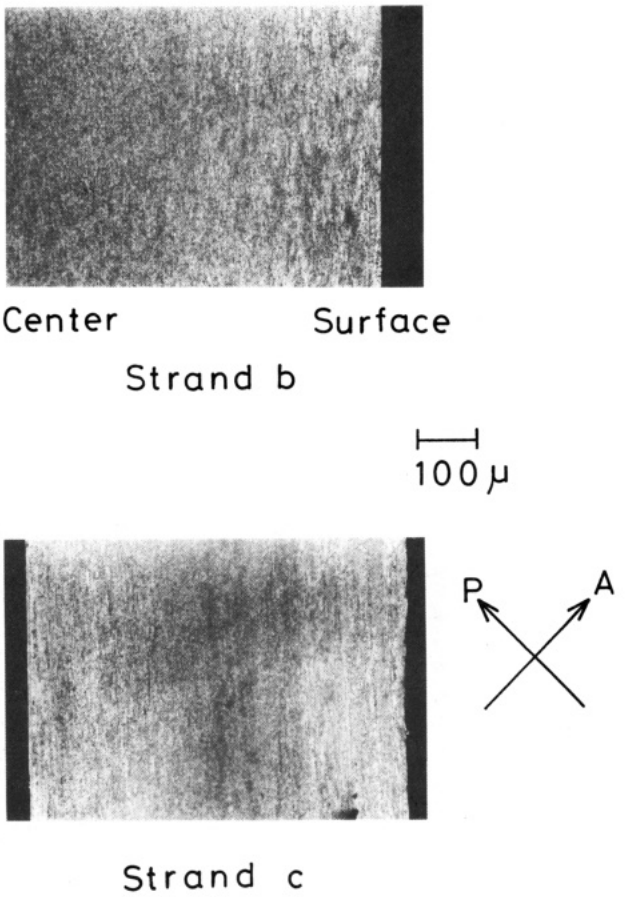

Figure 12. Polarized optical micrograph of strand b and strand c.

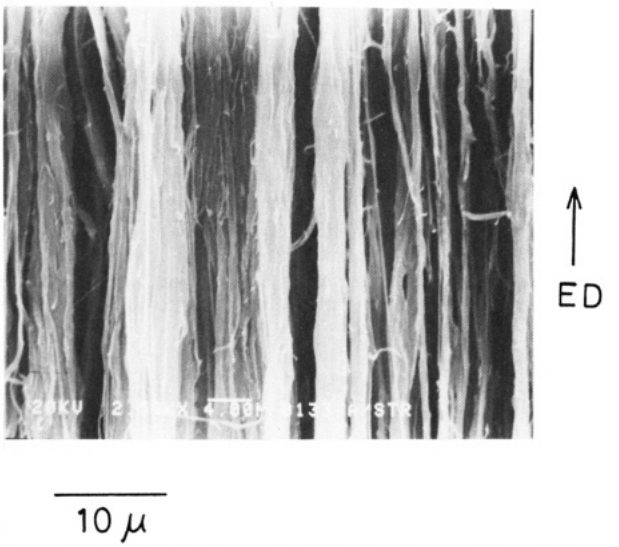

Figure 13. SEM photograph of the fracture surface of strand b.

the choice of image masking.[15,19,22] The use of single-image masking caused a drastic reduction in photometric accuracy.[15,19,22] The loss of photometric accuracy was considered to originate mainly from diffracted light and stray light from a neighboring hole. One of the ways to overcome such problems in the image masking is to use physical aperturing at the specimen[15] or dual-image masking.[19,20,22] Messerschmidt theoretically analyzed the effects of light diffraction on the performance of FTIR microspectroscopy and showed that the dual-image masking markedly reduced the effects of light diffraction.[19]

If spurious light is present, the 0% transmittance line must be lifted.[22] The liquid-crystalline polyester exhibits strong absorptions due to the CO stretching of the ether linkage in the wavenumber region of 1150–1300 cm^{-1}. The sample totally absorbed IR radiation in this spectral range and did not show any significant shift of the 0% transmittance line. From this observation, the FTIR microspectrum obtained by dual-aperture masking was considered to have sufficient photometric accuracy for the structural analysis of polymers.

We have recently discussed the applicability of FTIR microspectroscopy to the quantitative analysis of polymer samples.[23] We plotted the absorption intensity in the FTIR microspectrum against the film thickness and showed that Beer's law was valid in the absorbance range of 0–2.5. In addition, we confirmed that the polarization purity was retained in the measurement of FTIR microspectroscopy.[23] The dichroic spectra measured by the FTIR microspectroscopy were shown to agree with those obtained by the macroscopic transmission method.

Relationship between Microscopic Orientation and Bulk Orientation. The dichroic ratio of each molecular vibration can be related to the second moment of the orientation function of molecular chains. The orientation function of the transition moment f_i can be defined as

$$f_i = (R_i - 1)/(R_i + 2) \quad (1)$$

where R_i is the dichroic ratio of the ith vibrational mode.

Table II
Comparison of Bulk Orientation Function Obtained by FTIR Dichroism and WAXD

sample	orientation function	
	by FTIR dichroism	by WAXD
strand a	0.36–0.48	0.68
strand b	0.51–0.68	0.81
strand c	0.64–0.85	0.88
thin film	0.75–1.0	

The second moment of the chain-axis orientation function, f, can be calculated from f_i if the angle between transition moment and the chain axis, γ, is known.

$$f = f_i/f_0 \tag{2}$$

$$f_0 = (3\cos^2\gamma - 1)/2 \tag{3}$$

We measured the FTIR spectra for the highly oriented thin films of the liquid-crystalline polymer. For the 1474-cm^{-1} band, the observed value of f_i was 0.75, which provided the lower limits of the values of f_0 and f. The result shows that the transition moment angle of the 1474-cm^{-1} band is less than 24° and that the second moment of the chain orientation function of the thin film is higher than 0.75. The possible range of the orientation function of molecular chains can be evaluated from the dichroic ratio with the knowledge of the range of the transition moment angle ($\gamma < 24°$).

The microscopic orientation function obtained from FTIR microscopy can be related to the bulk orientation function by averaging over space

$$f_{bulk} = \int_0^{d/2} f(X)\, X\, dX / \int_0^{d/2} X\, dX \tag{4}$$

where $f(X)$ is the microscopic orientation function at the distance X from the center of the strand and d is the diameter of the strand. The possible range of the averaged orientation function of molecular chains is presented in Table II, as well as the crystal orientation function obtained from WAXD. The value of the crystal orientation function was shown to be higher than that of the averaged chain orientation function. The difference was more noticeable in the thicker strand. One of the possible explanations for the discrepancy is that there is a contribution to the infrared absorption bands from the noncrystalline region in which the molecular chains are less oriented than in the crystalline region. As the molecular chains become highly oriented to ED, the crystallinity of the polymer increases and the orientation function obtained by the IR dichroism approaches that determined by WAXD.

Relationship between Orientation Profile and Band Pattern Formation. The band pattern was observed only in the central region of strand a in which the lower degree of molecular orientation was revealed by the FTIR microscope. As the interval of the bands was about several micrometers, more than 20 layers were incorporated in the sample image of the FTIR microscope.

Takeuchi et al. studied the mechanism of band pattern development in shear-oriented thermotropic liquid-crystalline copolyester.[9] They concluded that the band pattern was developed by the residual longitudinal tension applied in the core layer during the cooling process and that the longitudinal stress was caused by the radial distribution of thermal and mechanical properties.[9] We also observed a similar band pattern in strand a, in which a large variation of the microscopic orientation function was observed in the radial direction. With an increase in the draw-down ratio and a decrease in the diameter of the strand, the orientation profile becomes more uniform, which also diminishes the radial distribution of thermal and mechanical properties. In the thinner strands with relatively uniform orientation profiles, the longitudinal stress is not sufficient for producing the band pattern.

Mechanism for the Formation of Skin–Core Structure. The skin–core structure of the thicker strand is considered to be formed by the flow history of the polymer melt. The flow of the molten polymers can be interpreted in terms of two types of basic flow; shear flow and elongational flow. As the gradient of flow velocity is much higher at the wall of die, the polymer melt flows at the wall with higher shear rate than at the center.[1,2] The shear flow may contribute to forming the highly oriented surface structure. On the other hand, it was reported that the elongational flow was more effective for orienting the rodlike molecules than the shear flow.[2] The velocity of the polymer flow was shown to be much lower near the wall than in the central region.[2] After leaving the die, the velocity profile becomes constant in the radial direction. As a result, the fluid element near the surface is stretched to a higher elongation than those in the central region in the draw-down process. The skin–core structure in the thicker strand is formed by these flow characteristics.At a higher draw-down ratio, however, the flow elements are stretched to a higher elongation even in the central region sufficiently enough to form a highly oriented texture.The effects of the diameter of the die on the orientation profile can be explained in an analogous way. When the diameter of the die decreases, the fluid elements are elongated to a higher ratio inside the die. The elongated polymer melts are solidified with retention of a high degree of molecular orientation.

Supplementary Material Available: Figures of sonic modulus as a function of diameter of strand, of bulk orientation function as a function of diameter of strand, and of FTIR spectra in the wavenumber region of 1000–600 cm^{-1} (3 pages). Ordering information is given on any current masthead page.

References and Notes

(1) Shimamura, K.; White, J. L.; Feller, J. F. *J. Appl. Polym. Sci.* **1981**, *26*, 2165.
(2) Ide, Y.; Ophir, Z. *Polym. Eng. Sci.* **1983**, *23*, 261.
(3) Sugiyama, H.; Lewis, D. N.; White, J. L.; Feller, J. F. *J. Appl. Polym. Sci.* **1985**, *30*, 2329.
(4) Muramatsu, H.; Krigbaum, W. R. *J. Polym. Sci., Polym. Phys. Ed.* **1986**, *24*, 1695.
(5) Krigbaum, W. R.; Liu, C. K.; Yang, D. K. *J. Polym. Sci., Polym. Phys. Ed.* **1988**, *26*, 1711.
(6) Itoyama, K. *J. Polym. Sci., Polym. Phys. Ed.* **1988**, *26*, 1863.
(7) Cuculo, J. A.; Chen, G.-Y. *J. Polym. Sci., Polym. Phys. Ed.* **1988**, *26*, 179.
(8) Chung, T.-S. *J. Polym. Sci., Polym. Lett. Ed.* **1986**, *24*, 299.
(9) Takeuchi, Y.; Shuto, Y.; Yamamoto, F. *Polymer* **1988**, *29*, 605.
(10) Itoyama, K.; Yamakawa, T. *Konunshi Ronbunshu* **1988**, *45*, 925.
(11) Itoyama, K. *J. Polym. Sci., Polym. Lett. Ed.* **1989**, *27*, 369.
(12) Weng, T.; Hiltner, A.; Baer, E. *J. Mater. Sci.* **1986**, *21*, 744.
(13) Blundell, D. J.; Chievers, R. A.; Curson, A. D.; Love, J. C.; MacDonald, W. A. *Polymer* **1988**, *29*, 1459.
(14) Pirnia, A.; Sung, C. S. P. *Macromolecules* **1988**, *21*, 2699.
(15) Chase, D. B. *ASTM Spec. Tech. Publ.* **1987**, *No. 949*, 4.
(16) Schearer, J. C.; Peter, D. C. *ASTM Spec. Tech. Publ.* **1987**, *No. 949*, 27.
(17) Bartick, E. G. *ASTM Spec. Tech. Publ.* **1987**, *No. 949*, 64.
(18) Mirabella, F. M., Jr. *ASTM Spec. Tech. Publ.* **1987**, *No. 949*, 74.
(19) Messerschmidt, R. G. *Microbeam Anal.* **1987**, *22*, 169.
(20) Reffner, J. A.; Messerschmidt, R. G.; Coates, J. P. *Microbeam Anal.* **1987**, *22*, 180.
(21) Bergin, F. J. *Appl. Spectrosc.* **1989**, *43*, 511.
(22) Ryan, J.; Kwiatkoski, J.; Reffner, J. A. *Am. Lab. (Fairfield, Conn.)* **1989**, *21*, 26.
(23) Kaito, A.; Nakayama, K., unpublished results.

Registry No. (HBA)(HNA) (copolymer), 81843-52-9.